Mitigation of ground motion effects in linear accelerators via feed-forward control

J. Pfingstner, K. Artoos, C. Charrondiere, St. Janssens,[†] M. Patecki,[‡] Y. Renier,[*]
D. Schulte, and R. Tomás

European Organization for Nuclear Research (CERN), Geneva 23, CH-1211, Switzerland

A. Jeremie

LAPP, Université de Savoie, 9 Chemin de Bellevue, 74941 Annecy-le-Vieux, France

K. Kubo, S. Kuroda, T. Naito, T. Okugi, T. Tauchi, and N. Terunuma

*High Energy Accelerator Research Organisation (KEK) and School of High Energy Accelerator Science,
Graduate University for Advanced Studies (SOKENDAI), 1-1 Oho, Tsukuba, Ibaraki 305-0801, Japan*
(Received 24 September 2014; published 4 December 2014)

Ground motion is a severe problem for many particle accelerators, since it excites beam oscillations, which decrease the beam quality and create beam-beam offset (at colliders). Orbit feedback systems can only compensate ground motion effects at frequencies significantly smaller than the beam repetition rate. In linear colliders, where the repetition rate is low, additional counter measures have to be put in place. For this reason, a ground motion mitigation method based on feed-forward control is presented in this paper. It has several advantages compared to other techniques (stabilization systems and intratrain feedback systems) such as cost reduction and potential performance improvement. An analytical model is presented that allows the derivation of hardware specification and performance estimates for a specific accelerator and ground motion model. At the Accelerator Test Facility (ATF2), ground motion sensors have been installed to verify the feasibility of important parts of the mitigation strategy. In experimental studies, it has been shown that beam excitations due to ground motion can be predicted from ground motion measurements on a pulse-to-pulse basis. Correlations of up to 80% between the estimated and measured orbit jitter have been observed. Additionally, an orbit jitter source was identified and has been removed, which halved the orbit jitter power at ATF2 and shows that the feed-forward scheme is also very useful for the detection of installation issues. We believe that the presented mitigation method has the potential to reduce costs and improve the performance of linear colliders and potentially other linear accelerators.

I. INTRODUCTION

The constantly increasing beam quality requirements cause modern particle accelerators to be more and more sensitive to ground motion effects [1,2]. Ground motion misaligns the accelerator components, most importantly quadrupole magnets that apply dipole kicks to the beam (feed-down effect). These unwanted dipole kicks excite beam oscillations that result in emittance increase due to chromatic dilutions [3,4], and in beam-beam offset at the interaction point in the case of colliders.

Without specially designed mitigation methods, these effects would reduce the performance of many modern accelerators significantly, or even prohibit their operation fully, as in the case of future linear colliders. Nowadays, orbit feedback systems [5] and transverse damping systems [6] are used to mitigate ground motion effects and other dynamic imperfections. The beam position is constantly measured via beam position monitors (BPMs) and actuations for corrector magnets are calculated that resteer the beam onto its reference orbit. The main limitation of such systems is that dynamic imperfections can only be suppressed if their frequencies are significantly smaller (factor 20 can be used as a rule of thumb) than the beam repetition rate f_R. This limit is due to considerations about the stability and noise amplification behavior of the applied feedback controllers. In rings, the repetition rate is usually much higher (kHz to MHz) than the relevant ground motion components (below 100 Hz), and the according beam oscillations can be damped. In linear accelerators, and especially in linear colliders, the repetition rate is much

[*]yves.renier@desy.de
[†]Also at Nikhef, Science Park 105, 1098 XG Amsterdam, The Netherlands.
[‡]Also at Warsaw University of Technology, Pl. Politechniki 1, 00-661 Warsaw, Poland.

lower than in rings. Important examples are the Compact Linear Collider (CLIC) [7,8] with 50 Hz, the International Linear Collider (ILC) with 5 Hz [9], and the Accelerator Test Facility (ATF2) [10,11] at KEK with 3.12 Hz. Because of these low repetition rates, orbit feedbacks are not sufficient to suppress all relevant ground motion effects and other mitigation methods have to be added for higher frequencies.

The topic of ground motion suppression for frequencies not correctable with orbit feedback systems (higher than about $f_R/20$) has already received significant attention. The problem has been addressed by intratrain feedback systems [12], which utilize ultrafast electronics to apply corrections within the same beam train. These systems are very efficient in removing the beam separation at the interaction point in the case of the ILC. However, the uncorrected beam oscillations in the main linac of the ILC create bunch distortions due to wakefield effects, which deteriorate the luminosity performance (banana effect). A fast luminosity feedback system has been considered to mitigate this effect [13], but it would be advantageous if the banana effect could be avoided in the first place.

In the case of CLIC, intratrain feedback systems are not sufficient to recover the design luminosity, since the bunch spacing is too short (0.5 ns) to react quickly enough. Also, the number of intratrain feedback systems that can be used in parallel at different locations is very limited, since the actions of the individual systems cannot be coordinated (local system). Because of these limitations, mechanical stabilization systems are currently the baseline for CLIC. They stabilize the quadrupole magnets themselves instead of steering the beam. Various active stabilization systems have been designed and tested [14–16]. Also a very effective passive stabilization system has been considered [17], but its large mechanical setup (100 ton concrete block and 20 air springs) limits its use to specific magnets, e.g., in the final focus system.

In this paper, a novel mitigation scheme for ground motion, or other mechanical vibration sources, with frequencies not correctable with orbit feedbacks is presented. It employs ground motion sensors, which cover the relevant frequency range, and which are distributed along the beam line. Their measurements are used to determine in real time the ground motion induced position change $x(t) = [x_1(t), ..., x_{N_q}(t)]^T$ of N_q quadrupole magnets. Either, each quadrupole is equipped with one ground motion sensor, or $x(t)$ is computed via interpolation from other sensor locations. The measured quadrupole motion $x(t)$ is then used to predict its effect on the beam orbit $b(t) = [b_1(t), ..., b_{N_B}(t)]^T$. This prediction is done with the help of a system model, more precisely the orbit response matrix R_q, as will be explained in Sec. III A. Finally, actuations $c(t)$ of corrector magnets are calculated that compensate $b(t)$, and these corrections are applied to the correctors in a feed-forward fashion. The feed-forward

system can only work effectively if the time response of the complete mitigation system [measurement, prediction of $b(t)$, calculation of $c(t)$, and actuation of the corrector magnets] is fast compared to the imperfections that should be corrected. Note that the beam orbit $b(t)$ is modeled as a continuous quantity. In reality the orbit is a time-discrete quantity $b_k = b(t_k)$, since it is only relevant at the beam arrival times $t_k = k/f_R$, where $k \in \{1, ..., N_P\}$ is the beam pulse index. For some explanations this detail will have to be considered.

The outlined feed-forward ground motion mitigation system has many advantages compared to the two other schemes. It is cheaper than active and passive stabilization systems due to the fact that no mechanical positioning or damping systems, e.g., tripods, are required. Even though the number of sensors will still be large, the number of corrector magnets can be reduced to a few very effective ones. Additionally, stabilization systems are more difficult to integrate into the complex accelerator modules. Compared to intratrain feedback systems, the feed-forward option has the advantage that it can apply corrections that are distributed over many correctors (global scheme). Therefore, beam oscillations can be damped already in the main linac before they filament and increase the beam emittance. This is especially important for CLIC, where the filamentation is strong due to the large energy spread, but is potentially also of interest for the ILC to suppress the banana effect. The efficiency of the feed-forward method is also not limited by very short bunch spacing, as is the case for CLIC.

Another advantage of the feed-forward scheme arises from the fact that all sensor measurements are available to one algorithm on a central computer that computes all the corrections. This is in contrast to other systems where each correction is computed on the basis of only one sensor, and no sensor information is exchanged between the independent subsystems. The additional information allows the use of a better optimized correction algorithm, e.g., by reducing the sensitivity to measurement noise. Also, more reliable error detection functionalities can be implemented. As a result the overall system can be made more robust, since the actions of erroneous sensors and correctors can be mitigated by other devices due to the global nature of the feed-forward scheme. On the other hand, the feed-forward system has high demands on the control system, since the data collection and the corrector actuation have to be performed with high speed to ensure an efficient mitigation. Besides the hardware specifications, the system model accuracy has to be higher compared to earlier schemes since usually the corrections are applied fully in each time step and not with a certain gain factor as in the feedback options. Another limitation for the effectiveness of the feed-forward method is that the real movements of the quadrupole magnet centere may differ from the movements predicted from the vibration sensor measurements,

depending where and how the vibration sensors are installed. Also, the feed-forward method is not capable of correction orbit changes from other sources than ground motion.

In Sec. II, an analytical model of the feed-forward scheme is presented. It can be used to investigate hardware limitations, and system specifications for the specific case of CLIC have been derived. Sections III and IV are concerned with the experimental demonstration of the feed-forward system. Since the full feasibility demonstration is a rather large project, the study was split into two parts: first, the prediction of the ground motion effect on the beam orbit; and second, the correction of the predicted orbit changes. Only the prediction part is covered in this paper while the demonstration of the correction part is planned in the near future.

To demonstrate the prediction part of the feed-forward mitigation scheme, experimental studies have been carried out at ATF2 and are presented in Sec. IV. ATF2 is an important test facility for the ILC, but also for CLIC, where recently the feasibility of an ILC-type beam delivery system was demonstrated [11]. The ATF2 beam line consists of an extraction line coming from the ATF damping ring, and a final focus region that focuses the beam to a nominal beam size of 37 nm in vertical direction. It is 82 m long and composed of 49 quadrupoles, 5 sextupoles, 4 skew sextuples, 7 dipoles, 3 septa, 25 corrector magnets, and different types of beam instrumentation equipment. Most importantly for this work are the 12 strip line BPMs at the beginning of the beam line and the 37 cavity BPMs further downstream (only 32 used for the experiment). The nominal electron beam has an energy of 1.3 GeV and horizontal and vertical emittances of 2 nm and 12 pm, respectively.

The conditions at ATF2 are very favorable for ground motion studies, since the beam line is relatively sensitive to these effects compared to other machines in operation. The necessary number of vibration sensors and their optimal locations were determined via previous simulation studies [18]. The simulations have also been used to evaluate the expected signal levels at ATF2 and therefore which prediction quality can be achieved. The results are presented in Sec. III.

II. MODELING OF THE MITIGATION CONCEPT

In this section, the analytical modeling of the feed-forward mitigation scheme is carried out. A frequency space model of the feed-forward mitigation scheme is derived in Sec. II A and is used in Sec. II B to predict the system performance and to determine hardware specifications. The model focuses on the correction part of the scheme, while the prediction part is assumed to work perfectly. It is assumed that the reader is familiar with the basic concepts of signal processing [19] and system

engineering [20] such as the Laplace transform and the $\mathcal{Z}$ transform.

A. System model

The simplified structure of the feed-forward mitigation system is depicted in Fig. 1. The ground motion $x_i(t)$ moves the magnetic center $m_i(t)$ of the quadrupole. The magnetic centers can also be changed by corrector magnets (actuators) $A(s)$, which are assumed to be integrated into the quadrupole magnets. In the expression $A(s)$, $s \in \mathbb{C}$ is the transformation variable of the Laplace transform. The corrector magnet is actuated by the feed-forward system that consists of a ground motion sensor $B(s)$ and time delay $D(s)$, where the latter is due to the control system and the correction algorithm. The measured signal is applied with a negative sign in order to cancel the effect of $x_i(t)$.

Since the feed-forward system can only correct motion above the lower cut-off frequency of the ground motion sensor, slower motion has to be corrected with an orbit feedback system. To get realistic performance estimates, the latter mitigation method is modeled in a simplified way. The feedback controller $C(z)$ is described as a discrete-time transfer function, via the $\mathcal{Z}$ transform with its transformation variable $z \in \mathbb{C}$. The $\mathcal{Z}$ transform is the equivalent to the Laplace transform for time-discrete signals. The feedback controller input is in this model the magnetic center $m_i(t)$, instead of the BPM reading. This simplification will be justified below. Note that the beam samples the position of the magnetic center with the time interval $T_R = 1/f_R$ (indicated in the plot with a switch symbol). This sampling transforms the continuous signal into a time-discrete series. The orbit feedback corrections are applied to the actuator $A(s)$ in addition to the feed-forward actuations. The fact that the output values of $C(z)$ are only changed in time intervals of T_R is modeled with a zero-order hold element.

The assumption and simplifications made in this model can be summarized as follows:

(1) The model is a single-input, single-output system (SISO) with only one quadrupole magnet, one BPM, and one actuator. The assumption is made that the real system (consisting of many elements) is as well
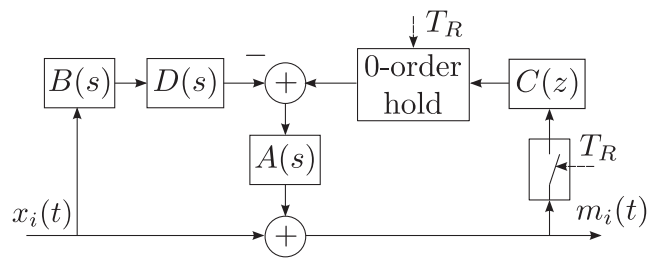

FIG. 1. Schematic diagram of the feed-forward mitigation system including an orbit feedback controller $C(z)$ for the suppression of relatively slow imperfections.

correctable as the SISO model, which requires very good system design and knowledge.

(2) The sensor is assumed to measure directly $x_i(t)$, which is only the case if the sensor is fixed to the quadrupole magnet, and the magnet is assumed to be perfectly rigid.

(3) Also, the corrector magnet is assumed to be installed directly in the quadrupole magnet. In reality, only a small number of very effective correctors may be used to steer the beam and not every quadrupole will have to be equipped with a corrector magnet.

(4) In the model, the input of $C(z)$ is the magnetic center $m_i(t)$ directly, while in reality the BPM readings are used. This assumes that the orbit prediction part of the mitigation scheme works perfectly.

Considering Fig. 1, the frequency response $S(i\omega)$ of $m_i(t)$ to $x_i(t)$ can be shown to be

$$S(i\omega) = S_{FF}(i\omega)S_{OF}(e^{i\omega T_R}) \tag{1}$$

with

$$S_{FF}(i\omega) = 1 - B(s)D(s)A(s)|_{s=i\omega}, \tag{2}$$

$$S_{OF}(e^{i\omega T_R}) = \frac{1}{1 + C(z)A(z)}\Bigg|_{z=e^{i\omega T_R}}, \tag{3}$$

where $S_{FF}(i\omega)$ and $S_{OF}(e^{i\omega T_R})$ are the frequency responses of the feed-forward and the orbit feedback system, respectively. Note the combination of continuous and time-discrete signals. As known from signal theory, the transformation variables of the Laplace and $\mathcal{Z}$ transform have to be evaluated on the imaginary axis and around the unit circle of the complex plane, respectively, to obtain the according frequency response functions. The model is also capable of investigating the performance of stabilization systems, by simply exchanging $S_{FF}(i\omega)$ in Eq. (2) with the according stabilization frequency response, as done in [21]. The time-discrete actuator $A(z)$ corresponds to the continuous actuator $A(s)$ with a zero-order hold element at its input and a sampling device at its output. The behavior of $A(z)$ can be derived from $A(s)$ by performing the so-called ζ transform, which is given by (see [21,22] for detailed information)

$$A(z) = (1 - z^{-1})\mathcal{Z}\left\{\mathcal{L}^{-1}\left\{\frac{A(s)}{s}\right\}\Bigg|_{t=kT_R}\right\}. \tag{4}$$

B. Performance predictions

For the performance predictions, two different sensor types are considered. The seismometer CMG-6T [23] from Guralp, with its transfer function $B_1(s)$, has a lower and upper cutoff frequency of 0.03 Hz and 100 Hz, respectively. The second transfer function $B_2(s)$ corresponds to a

geophone proposed by the CLIC stabilization group [24]. The geophone's lower cutoff frequency is 0.9 Hz and it can measure up to 1 kHz. The geophone would be significantly cheaper than the seismometer and efforts are ongoing to build a prototype of this instrument. For background information about the different types of vibration sensors, please refer to [25].

Also two different types of actuators have been considered

$$A_1(s) = \frac{1}{1 + T_1 s} \quad \text{and} \quad A_2(s) = \frac{1}{(1 + T_1 s)^2}, \tag{5}$$

where $A_1(s)$ and $A_2(s)$ correspond to a first and second order low-pass behavior with adiabatic damping, respectively. The time constant T_1 corresponds to the time to reach 63.2% of the amplitude of an applied step function. In Eq. (3), the time-discrete equivalent of these continuous actuator dynamics is also needed. Using the ζ transform in Eq. (4), they can be shown to be

$$A_1(z) = \frac{1 - e^{-\frac{T_R}{T_1}}}{z - e^{-\frac{T_d}{T_1}}} \quad \text{and} \tag{6}$$

$$A_2(z) = \frac{1 - e^{-\frac{T_R}{T_1}}}{z - e^{-\frac{T_d}{T_1}}} - \frac{T_R}{T_1}\frac{(z-1)e^{-\frac{T_R}{T_1}}}{\left(z - e^{-\frac{T_R}{T_1}}\right)^2}. \tag{7}$$

The time delay T_t can be modeled in frequency space as

$$D(i\omega) = e^{-i\omega T_t}, \tag{8}$$

and the simplified action of the orbit controller is modeled as a discrete-time integrator given by

$$C(z) = \frac{z}{z - 1}. \tag{9}$$

The impact of ground motion with respect to a specific accelerator quantity, e.g., emittance increase, luminosity loss, or orbit offset, can be estimated with an analytic model that is developed in [2]. Including also the action of the feed-forward system and the orbit feedback system, but neglecting a possible intratrain feedback system, the luminosity loss $\Delta\mathcal{L}$ can be modeled as

$$\Delta\mathcal{L} = \frac{1}{(2\pi)^2}\iint_{-\infty}^{\infty} G_{\mathcal{L}}^2(k)|S(i\omega)|^2 P(\omega, k)\,d\omega dk. \tag{10}$$

The ground motion $P(\omega, k)$ is modeled via the two-dimensional power spectral density (PSD), which is a function of the angular frequency $\omega = 2\pi f$, but also includes spatial properties via the wave number $k = 2\pi/\lambda$. Here f and λ are the frequency and the wavelength of a ground motion wave. Many different models for $P(\omega, k)$ are available in the literature. In this work, the model B10 [26] is used, which is the baseline model for CLIC. It is an adaptation of the standard model B (moderate

ground motion), but has stronger cultural noise components (by a factor 10) to fit recent measurements. The PSD defines the power of independent sine waves $\sin[\omega t - ks + \phi_0(\omega, k)]$, where s is the spatial coordinate and $\phi_0(\omega, k)$ is a random phase. The power of the exciting ground motion is related to the motion of the magnetic center $m_i(t)$ of the quadrupole magnets via $|S(i\omega)|^2$ [see Eq. (1)] if the action of the feed-forward and orbit feedback system is taken into account. Finally, the motion of the magnetic centers is related to the luminosity loss via the sensitivity function $G_{\mathcal{L}}^2(k)$, which can be determined from simulations. The power of the individual sine waves (different ω and k) is added up via double integration. More details can be found in [21].

In Fig. 2 the dependence of the feed-forward system performance on the actuator dynamics is shown. It can be seen that the first-order actuator dynamics $A_1(s)$ are strongly preferable compared to the second-order dynamics of $A_2(s)$. Also, the Guralp seismometer $B_1(s)$ performs better than the geophone $B_2(s)$, which is in contrast to the application of the sensors to stabilization systems. To keep the luminosity loss below 2%, T_1 should be below 2 ms for $B_2(s)$ and between 2 ms and 5 ms for $B_1(s)$.

Surprisingly, the use of sensor $B_1(s)$ results in an increased luminosity loss for actuator dynamics below 2 ms. To understand this behavior the integrated root mean square (RMS) relative luminosity loss for different configurations of mitigation methods is depicted in Fig. 3, which can be calculated as

$$\frac{\Delta\mathcal{L}(\omega)}{\mathcal{L}_0} = \frac{2}{(2\pi)^2\mathcal{L}_0}\int\limits_{\bar{\omega}=\omega}^{\infty}\int\limits_{k=-\infty}^{\infty} G_{\mathcal{L}}^2(k)|S(i\bar{\omega})|^2 P(\bar{\omega}, k)\mathrm{d}\bar{\omega}\mathrm{d}k.$$
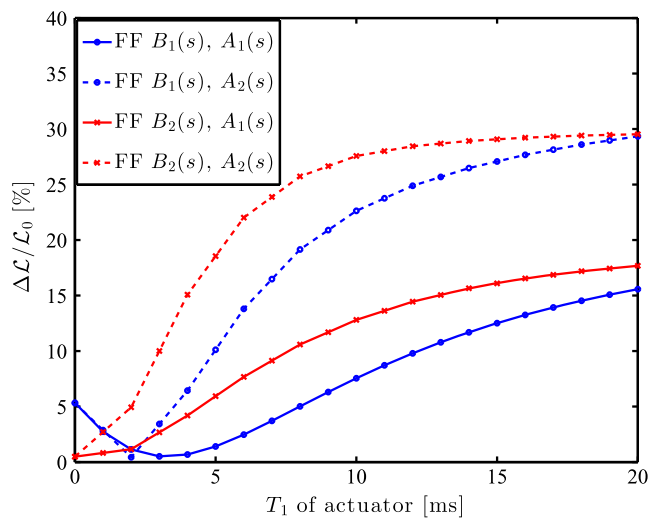
(11)

FIG. 2. Relative luminosity loss with the feed-forward and orbit feedback system with respect to the actuator dynamics for the case of CLIC.
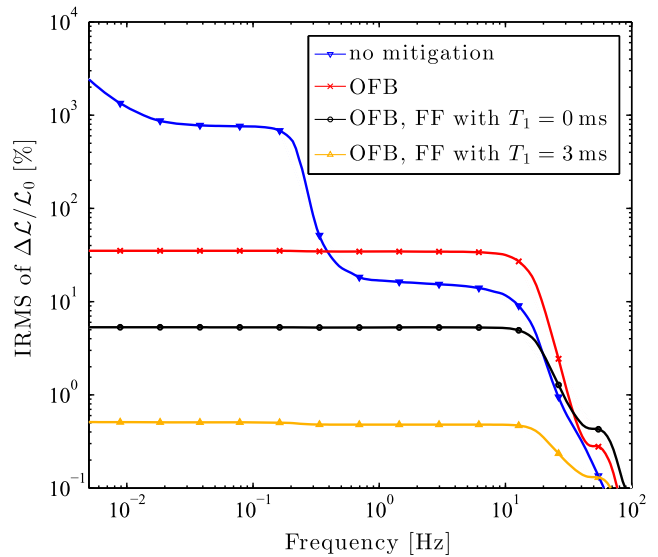

FIG. 3. Integrated root mean square of the relative luminosity loss $\Delta\mathcal{L}/\mathcal{L}_0$ including the effect of the orbit feedback system (OFB) and the feed-forward system (FF).

The additional factor 2 compared to Eq. (10) comes from the fact that the integration over $\bar{\omega}$ is only carried out for positive values. Without any mitigation methods, the luminosity decreases strongly for frequencies below 0.5 Hz. The plotted luminosity losses higher than 100% are due to the limitations of the used model, which is only accurate for losses below 40%. However, the curves still indicate frequency ranges causing high luminosity loss. When using an orbit feedback, the luminosity loss can be limited to about 35%. The remaining loss is mainly caused by ground motion of frequencies between 10 Hz and 50 Hz. These frequencies can be mitigates by the use of the feed-forward system [first-order actuator $A_1(s)$ and Guralp seismometer $B_1(s)$]. The system suppresses higher frequencies more efficiently with an actuator with low-pass behavior (T_1 of 3 ms) than with an ideal actuator (T_1 of 0 ms). This is due to the fact that the low-pass behavior compensates partially the strong phase distortions of the seismometer $B_1(s)$, which turns out to be beneficial for the real-time control. For the geophone $B_2(s)$ such an effect is not observable, since the phase distortions of this sensor are smaller at high frequencies.

The dependence of the performance of the feed-forward system on the system delay T_t is depicted in Fig. 4. Since actuator $A_1(s)$ has already turned out to be superior compared to $A_2(s)$, only the former one is used for the evaluation. As expected, an infinitely fast actuator ($T_1 = 0$) performs in general better than one with realistic dynamics. To limit the luminosity loss below 5% (instead of 2%, since now two imperfections are considered), the delay time T_t has to be below 1 ms for $B_2(s)$ and 4 ms for $B_1(s)$, when assuming an actuator time constant T_1 of 3 ms.
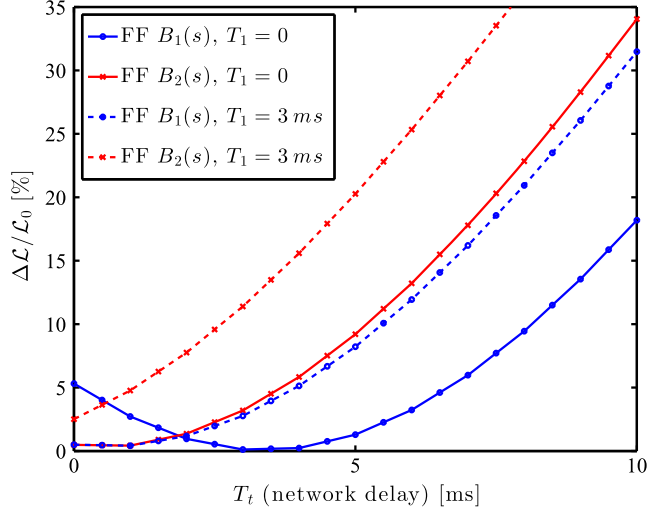
FIG. 4.   Relative luminosity loss with the feed-forward and orbit feedback system as a function of the system delays for the case of CLIC. Only a perfect actuator ($T_1 = 0$ ms) and $A_1(s)$ with $T_1 = 3$ ms are considered.

III. SIMULATION STUDIES FOR THE EXPERIMENT AT ATF2

Since the experimental conditions at ATF2 are very different compared to the case of future linear colliders, simulation studies have been performed (see also [18]) to evaluate the expected performance of the feed-forward mitigation method. Even though ATF2 is relatively sensitive to ground motion, the expected effects are still small compared to the measured orbit changes originating from other imperfections. Therefore, it has to be verified if an experiment is feasible.

A. Tools, models, and data processing

The simulations have been performed with the tracking code PLACET [27] and in parallel with the ATF2 Flight Simulator [28]. The results have been checked against each other and only negligible differences could be observed. The beam was tracked through the lattice of version 5.1, which corresponds to the nominal beam optics with the horizontal beta function increased at the interaction point by a factor 10, which was in use at the time the experiment was conducted.

To evaluate the effect of ground motion on the beam orbit, a ground motion generator was used to create realistic element misalignments on a pulse-to-pulse basis. The generator originates from the work in [2] and has been integrated into PLACET [26]. The applied ground motion model has been established from measurements along the ATF2 beam line [29]. To simulate the measurement, seismometers of the type Guralp CMG-6T have been added to the beam line. Two different setups are utilized to evaluate the necessary number of sensors: one with 14 and one with 30 seismometers. The locations of these

sensors have been determined (more details later) in order to best cover the areas in which most orbit jitter (due to ground motion) is created.

Besides the pulse-to-pulse ground motion, other imperfections have been included. Field errors of the quadrupole magnets of 0.01% and BPM scaling errors of 1% have been modeled. The BPM resolution was set to 5 μm for the stripline BPMs (beginning of the beam line) and to 0.1 μm for the cavity BPMs (further downstream in the final focus region). Also, initial orbit jitter with an amplitude of 10% and 25% of the beam size in horizontal and vertical direction, respectively, have been included in the simulations. This is consistent with current measurements [30]. The sextupole magnets in the final focus region were turned off during the whole simulation (as in the experiment) to avoid nonlinear effects due to large orbit changes.

As a first step in the simulation procedure, the initial survey is modeled. All quadrupole magnets and BPMs are misaligned with Gaussian noise of zero mean and with a standard deviation of 100 μm. Afterwards, the beam orbit is steered with the corrector magnets to the center of the BPMs. Next, the orbit response matrix $\boldsymbol{R}_q$ is computed. The elements of this matrix are orbit changes at the BPM locations due to quadrupole misalignments in linear approximation: $r_{ij} = db_{ik}/dx_j$. The main part of the simulation consists of tracking 200 beam pulses, while applying ground motion and the other imperfections. The resulting sensor and BPM readings are recorded and processed as discussed below. To acquire sufficient statistics, the results of 20 random seeds have been averaged.

The numerical tool Octave [31] was used for the processing of the simulation data. The original BPM readings $\boldsymbol{b}_k$ are not analyzed, where $k \in \{1, ..., N_P\}$ is the pulse index. Instead, the difference between two beam pulses $\Delta\boldsymbol{b}_k = \boldsymbol{b}_k - \boldsymbol{b}_{k-1}$ is used, which is referred to in the following as orbit jitter. Using the orbit difference corresponds to the application of a high-pass filter to the original data. This allows one to suppress the influence of lower frequencies that would be corrected by an orbit feedback system in reality.

The vibration sensor measurements at the beam arrival times are used to find the estimated position changes $\Delta\hat{\boldsymbol{x}}_k$ of all quadrupole magnets. Since the locations of the quadrupole magnets and vibration sensors are not always the same, the quadrupole magnet positions are determined via linear interpolation from the sensor measurements. Other interpolation methods, e.g., cubic or spline interpolation, did not reduce the position errors noticeably and were less reliable. The interpolated quadrupole jitter $\Delta\hat{\boldsymbol{x}}_k$ is then used to predict the ground motion effect on the beam orbit $\Delta\hat{\boldsymbol{b}}_k$ by

$$\Delta\hat{\boldsymbol{b}}_k = \boldsymbol{R}_q \Delta\hat{\boldsymbol{x}}_k. \tag{12}$$

For the following explanations, it is convenient to combine the orbit jitter of all BPMs and time steps (1 to N_P) in one matrix

$$\Delta \boldsymbol{B} = \begin{bmatrix} \Delta \boldsymbol{b}_1^T \\ \vdots \\ \Delta \boldsymbol{b}_{N_P}^T \end{bmatrix}. \quad (13)$$

In the same way, $\Delta \hat{\boldsymbol{B}}$ can also be formed out of the ground motion effect predictions $\Delta \hat{\boldsymbol{b}}_k$. The ith column of $\Delta \hat{\boldsymbol{B}}$ corresponds to the effect in the ith BPM and will be referred to in the following as $\Delta \hat{\boldsymbol{B}}_i$.

Using this definition, it can be quantified how well the ground motion effect predictions can be observed at ATF2. As a measure, the correlation coefficient r is utilized, which is given for the ith BPM by

$$r_i = \frac{\mathrm{cov}(\Delta \boldsymbol{B}_i, \Delta \hat{\boldsymbol{B}}_i)}{\sigma(\Delta \boldsymbol{B}_i)\sigma(\Delta \hat{\boldsymbol{B}}_i)}, \quad (14)$$

where $\sigma(\boldsymbol{b}_i)$ is the standard deviation of any vector $\boldsymbol{b}_i$, and $\mathrm{cov}(\boldsymbol{b}_i, \boldsymbol{b}_j)$ is the covariance of two vectors given by

$$\mathrm{cov}(\boldsymbol{b}_i, \boldsymbol{b}_j) = \frac{1}{N-1} \sum_{k=1}^N (\boldsymbol{b}_i[k] - \bar{\boldsymbol{b}}_i)(\boldsymbol{b}_j[k] - \bar{\boldsymbol{b}}_j). \quad (15)$$

In this expression, $\bar{\boldsymbol{b}}_i$ symbolizes the mean value of $\boldsymbol{b}_i$. The correlation coefficient r of two signals is equal to 1 (or -1) if the signals are fully linearly dependent. If the two signals are statistically independent, the correlation coefficient is 0.

B. Results

Figure 5 shows the contribution of ground motion and BPM noise to the overall vertical RMS orbit jitter, which is currently observed, by considering the effects independently in simulations. In the beginning of the beam line (lower BPM numbers), the BPM noise is much larger than the orbit jitter due to ground motion. In this area, the strip line BPMs with a resolution of about 5 μm are used, with the exception of the three cavity BPMs (numbers 10, 11, and 12). Further downstream in the final focus region (higher BPM numbers) the ground motion effect becomes larger and the BPM noise smaller (cavity BPMs with 0.1 μm resolution are used [32]). Only this region is sensitive enough for the ground motion effect prediction, since the ground motion effect is large compared to the BPM resolution. The BPM with number 34 has a low sensitivity, due to the low beta function at the location of this instrument. This will be considered in the data analysis, by excluding this device.

Even though the BPM noise in the sensitive region is significantly lower than the ground motion effect [30], the
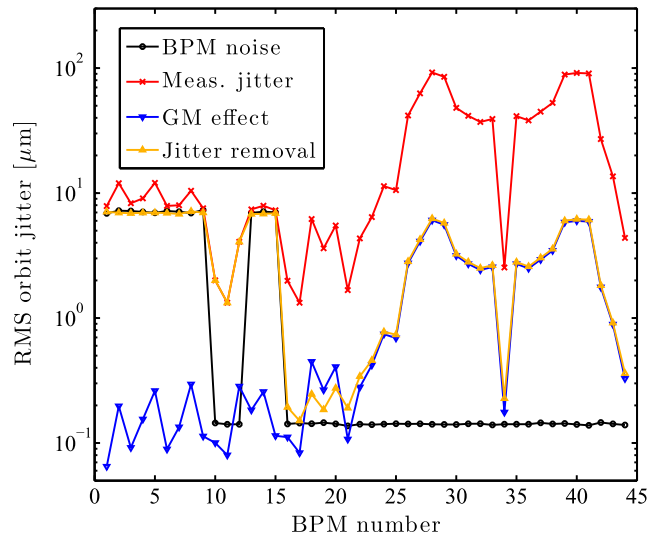

FIG. 5. Vertical RMS orbit jitter at the BPM locations due to different contributions compared to the BPM noise.

measured orbit jitter [30] is still much larger than the orbit jitter induced by ground motion. The signal levels differ by a factor 100 and 20 in horizontal and vertical direction, respectively. This fact poses significant problems for the experiment at ATF2. Even if the ground motion effect could be perfectly predicted from the sensor readings, hardly any correlation with the BPM readings would be observed, since the ground motion effect is very small compared to the full orbit jitter.

To overcome this problem a technique was developed that is capable of subtracting most of the incoming orbit jitter (which is assumed to come from other sources than ground motion) from the downstream BPM measurements. This technique is based on the assumption that the ground motion effects are (according to simulations) still very low at the locations of the three upstream high-resolution cavity BPMs (number 10, 11, and 12, located just after the quadrupole magnets QD10X, QF11X, and QD12X), where the incoming parasitic orbit jitter can be well observed. Therefore, all downstream BPM data are decorrelated from the measurements of the mentioned three BPMs in order to subtract the incoming beam jitter. In [33], it is shown that such a decorrelation of a BPM data set $\Delta \boldsymbol{B}_i$ from another set of BPM data $\Delta \boldsymbol{B}_{up}$ is given by

$$\Delta \boldsymbol{B}_i^{(r)} = \Delta \boldsymbol{B}_i - \boldsymbol{K}_{up} \Delta \boldsymbol{B}_i, \quad (16)$$

$$\boldsymbol{K}_{up} = \Delta \boldsymbol{B}_{up} \Delta \boldsymbol{B}_{up}^\dagger, \quad (17)$$

$$\Delta \boldsymbol{B}_{up} = [\Delta \boldsymbol{B}_{10}, \Delta \boldsymbol{B}_{11}, \Delta \boldsymbol{B}_{12}], \quad (18)$$

where $\Delta \boldsymbol{B}_i^{(r)}$ are the decorrelated data, and † symbolizes the pseudoinverse of a matrix. After applying the jitter removal, the RMS values of the decorrelated orbit jitter
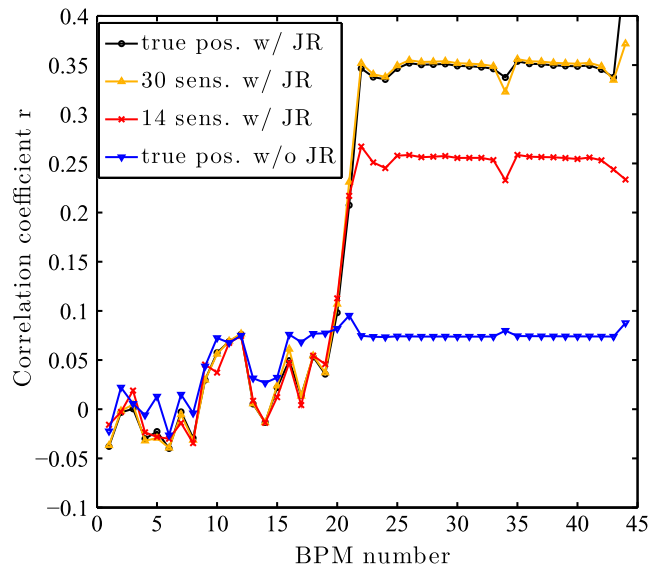
FIG. 6. Correlation coefficient r calculated from the BPM readings and the predicted ground motion effect for the vertical direction. For the prediction of the ground motion effect, either the true quadrupole positions have been used, or the positions are interpolated from the readings of 14 or 30 vibration sensors. Also the result with the orbit jitter after removal of the incoming orbit jitter (JR) is shown.

FIG. 7. Correlation coefficient r at the BPM locations along the beam line in horizontal direction. The prediction results for known quadrupole positions (true pos.) are shown with and without removal of the incoming orbit jitter (JR).

are close to the ones of the ground motion induced orbit jitter (see Fig. 5).

In Fig. 6, the simulated correlation coefficients r [see Eq. (14)] are shown first for the vertical direction. Up to BPM 20, r is very low and no clear signal dependence can be observed. This is due to the small ground motion effect and the large BPM noise. Downstream of BPM 20, consistent correlation with a value of 0.25 can be observed if 14 seismometers are used. If 30 seismometers are installed, r increases to 0.35. This is basically the same result as with true quadrupole position knowledge. The mentioned correlation values can only be reached when the incoming beam jitter is removed according to Eqs. (16)–(18). Without the application of this procedure, only correlation of 0.07 can be observed. The correlation coefficient r for the horizontal direction is depicted in Fig. 7. In general, the correlation values are smaller than in the vertical direction. This is specially true for the option with 14 vibration sensors. In both directions, the values of the correlation coefficients are limited by the measurement noise of the BPMs that are used for the orbit jitter removal.

From these simulations, it can be concluded that due to the small ground motion effect on the orbit jitter compared to other orbit jitter sources, only relatively small correlation values can be expected, and the removal of incoming beam jitter is necessary. This is in contrast to the situation at future linear colliders, where the ground motion effect is the most important jitter source. However, the sensitivity in the final focus region in the vertical direction seems to be high
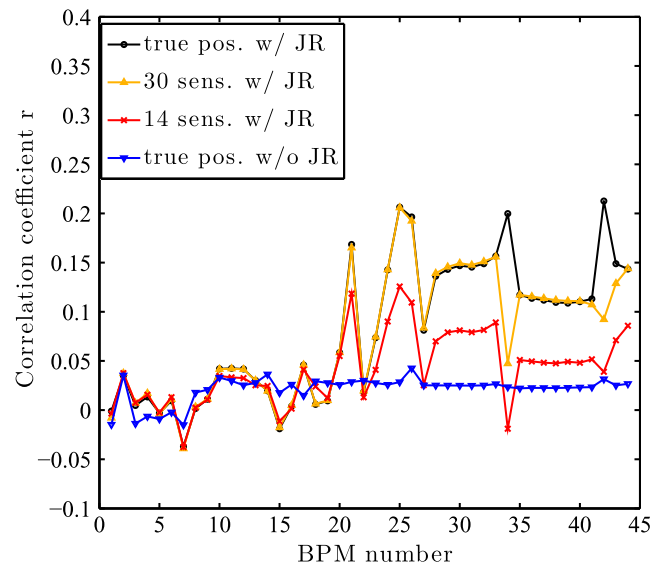
enough to justify the experiment. Using 14 seismometers is enough to predict the quadrupole magnet motion to a sufficient level. The locations of these sensors, listed in Table I, have been chosen to be close to the quadrupole magnets that are most sensitive to misalignments with respect to their effect on the beam orbit. This sensitivity can be studied by comparing the standard deviations of the columns of the orbit response matrix $\boldsymbol{R}_q$. An exception to this choice is sensor S14, which is placed next to QD0FF, which is the last magnet of the beam line. To monitor its vibration is important, since it can create significant orbit jitter at the interaction point, which cannot be observed by any currently operating BPMs.

It should be mentioned, however, that the experiment relies on an efficient removal of the orbit jitter from other

TABLE I. Overview of the 14 chosen sensor locations.

Sensor name	Sensor location	Distance from sensor S1
S1	on QF1X	0 m
S2	on QD2X	2.0 m
S3	beside QF3X	3.0 m
S4	beside QF4X	7.3 m
S5	beside QD5X	8.2 m
S6	beside QF11X	22.0 m
S7	beside QD12X	23.4 m
S8	beside QF13X	24.5 m
S9	beside QD14X	25.5 m
S10	beside QF15X	26.5 m
S11	beside QD16X	27.6 m
S12	beside QD18X	31.4 m
S13	beside QD19X	32.4 m
S14	beside QD0FF	80.8 m

sources than ground motion. The developed removal technique only works if this parasitic orbit jitter is produced upstream of the BPMs used for the jitter subtraction, which are located around sensor 6 and 7. This assumption, in combination with the expected small correlation values of only 0.25, makes the experimental prediction of the ground motion effect (presented in the next section) a very challenging task.

IV. EXPERIMENTAL STUDIES AT ATF2

In this section, the experimental demonstration of the prediction of ground motion effects from vibration sensor measurements are presented. The experiments have been conducted at ATF2 [10] at KEK. The ATF2 beam line is very well suited for ground motion experiments due to its relatively high sensitivity compared to other machines. This sensitivity to ground motion effects originates from the very small beam emittances. Additionally, the available high-resolution BPM system makes it possible to observe the small transverse beam oscillations induced by ground motion.

A. Measurement setup and data analysis

The experimental setup at ATF2 is depicted in Fig. 8. It consists of three parts: (1) BPM system to measure the orbit jitter; (2) ground motion data acquisition system; and (3) synchronization signal.

Two types of BPMs are installed: strip line BPMs and cavity BPMs. For the experiment mainly the cavity BPMs [32] are used, since the stripline BPMs are not sensitive enough for the ground motion effects. The BPM data are made available via the distributed control system EPICS [34]. The collected data are then used in the offline data analysis.

To measure the ground motion vibrations, 14 seismometers (GM) of the type CMG-6T from Guralp have been installed along the beam line. These seismometers are specified to measure in a frequency range from 0.03 Hz to

100 Hz [23]. The number and the locations of the sensors have been chosen with the help of simulations (see Sec. III). The seismometers have been either installed directly on top of certain quadrupole magnets, or close to them depending on the available space and security considerations (see Table I for details). The vibration sensors are connected via well shielded cables to a National Instruments controller of the type PXI 8109 RT. This device is equipped with the digitizer card 6289, also from National Instruments. Here the analog vibration signals in the horizontal and vertical direction are recorded. A Labview program was developed that controls the acquisition process. The stored ground motion data are used in the offline analysis together with the BPM data. It should be mentioned that below 0.2 Hz, the sensor noise contributions are high [25]. Therefore, lower frequencies have been suppressed by applying a second-order Butterworth high-pass filter in the offline analysis.

The BPM measurements are triggered by the beam arrival that occurs at a repetition rate f_R of 3.12 Hz. The ground motion digitization, on the other hand, is triggered by the internal clock of the National Instruments at a repetition rate of 1024 Hz. It is necessary to select the recorded ground motion data that are closest in time to the beam arrival times. Therefore, a synchronization signal was set up that is also recorded by the National Instruments digitizer. The synchronization signal indicates the beam arrival time, and it is used for the ground motion data selection.

To achieve a secure synchronization the experiment is conducted in the following way. The beam is only turned on after the data acquisitions of the BPMs and ground motion sensors with synchronization signal have already been started. This switching on of the beam is clearly visible in the data of both measurement systems, due to the following reasons. In the BPM system, the missing beam will result in very large measurement noise that can be easily identified in the offline analysis. With the National Instruments equipment, the ground motion measurements as well as the synchronization signal are recorded. As is shown in Fig. 8, the synchronization signal has pulses at the kicker trigger times, only if the beam charge is above a certain threshold value. In the offline analysis, these recorded pulses can be detected and the corresponding ground motion data can be extracted (downsampling from 1024 Hz to 3.12 Hz).

Before the end of the data acquisition the beam is turned off, which leaves a second clear signature in the measurement data. In the offline analysis, the data with beam presence can be selected. Some additional tests are performed to verify the consistency of the data. Afterwards, the orbit jitter due to ground motion is predicted from the seismometer measurements. Finally the predictions are compared with the real measurements with the help of the correlation coefficient, for details see Sec. III.
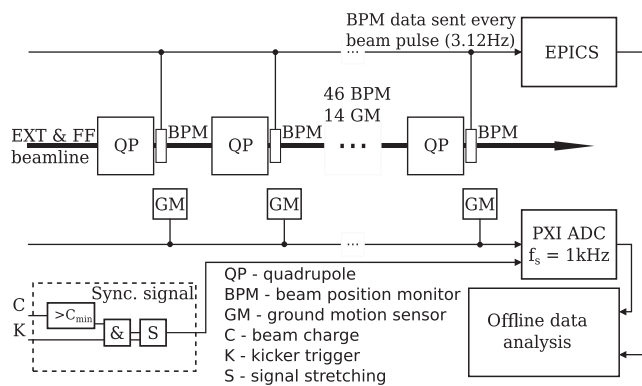

FIG. 8.   Overview of the experimental setup at ATF2. The beam passes from left to right through the quadrupole magnets and BPMs.

B. Ground motion measurements

The seismometer recordings over 20 min have been used to calculate its power spectral density and its integrated root mean square motion. The results are depicted in Figs. 9 and 10 for three different sensors. Each PSD is calculated with Welch's method [35] and the IRMS is created via an integration of the power density (see [21] for more details). The measurements are compared with the ground motion model of type ATF2, which has been used for the simulation studies in Sec. III. The location of the sensors and their distance from each other are given in Table I.

The PSDs of the sensors 7 and 14 are very similar, as it is also the case for all sensors that are not plotted. The measurements also fit well with the model, even though the real vibrations are slightly weaker than expected in the frequency range from 2 to 6 Hz. A deviation in this frequency range is normal, since the corresponding vibrations are created by changing crustal motion (crustal resonance). Also below 0.2 Hz, the measurements deviate from the model, since the seismometer cannot measure below this frequency. The corresponding motion is however of little importance for the experiment. This is mainly due to the fact that the impact of slow movements get suppressed strongly by the use of the differential motion between two beam arrivals $\Delta \hat{x}_k$ for the correlation studies instead of $\hat{x}_k$. Only the motion measured by sensor 2 deviates strongly from the data of the other sensors. Strongly increased vibrations in a broad frequency range from 8 Hz to about 100 Hz are observed that have two pronounced maxima at 9.94 Hz and 24.25 Hz. This strong motion localized around sensor 2 was unexpected and has not been included in the simulation studies in Sec. III. Therefore, the ground motion effect at ATF2 is probably stronger than
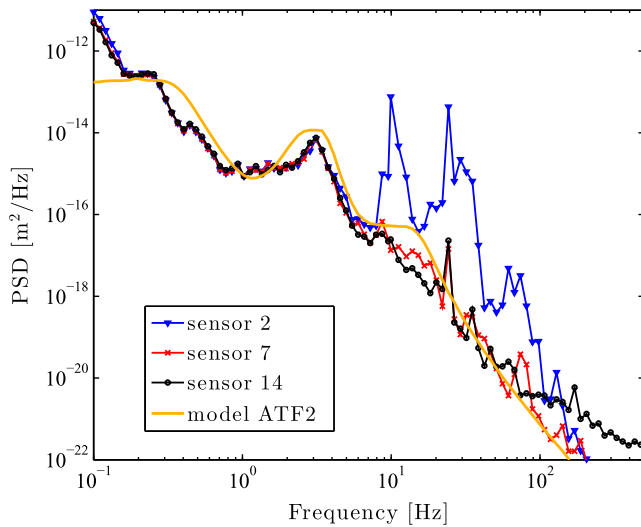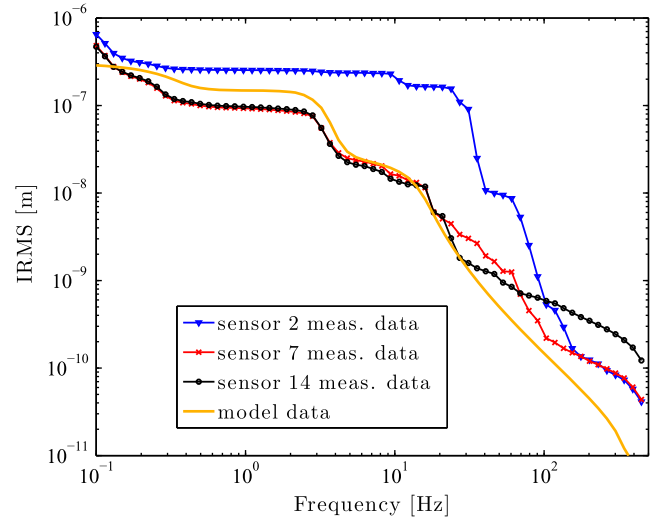

FIG. 10. Integrated root mean square motion (IRMS) of the ground motion sensor measurements and model data in vertical direction.

predicted. This surprising finding also indicates that there are strong ground motion contributions from the beginning of the beam line. Therefore, the removal of the incoming jitter [according to Eqs. (16)–(18)] might not work as expected, since the BPMs used by the removal procedure are located further downstream around sensor 6 and 7 (as in the simulations).

In Fig. 11 the correlation spectra (see [2] for a definition) of sensor 1 with three other sensors are depicted and compared to model predictions. The distances of these sensors from each other are listed in Table I. It can be seen that for frequencies below 0.2 Hz the correlation drops quickly due to the large noise content in the seismometer
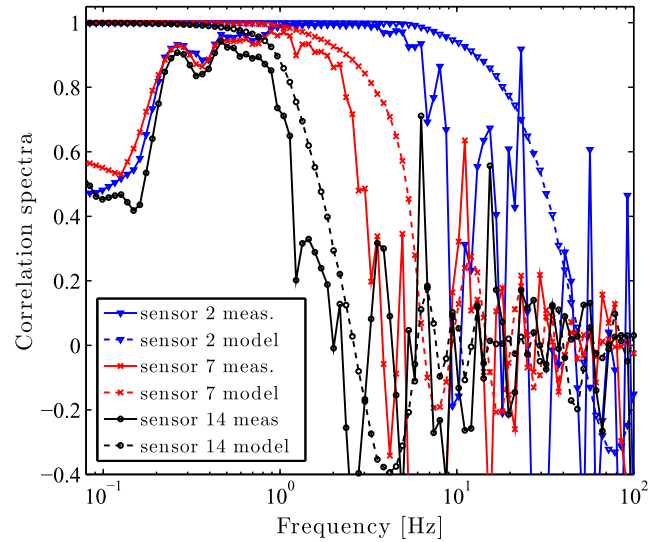

FIG. 9. Power spectral densities of the ground motion sensor measurements and model data in vertical direction.

FIG. 11. Correlation spectra of the ground motion sensor 1 with other sensors' measurements in vertical direction. The measurements are compared with model predictions.

measurements. At higher frequencies, the measurements show lower correlation than predicted by the model. A possible explanation for this model mismatch could be that the ground motion behavior has changed since the generation of the model, e.g., due to earth settlements or earthquakes. For sensor 2 in particular the measured correlation drops at much lower frequencies than the corresponding model, but this is due to the additional unpredicted vibrations observable in Fig. 9.

C. Correlation studies

The seismometer measurements are used to predict their effect on the orbit jitter according to Eq. (12). The predictions are then compared with the BPM data with the help of the correlation coefficient [introduced in Eq. (14)]. The data sets were acquired in parallel for about 15 min. Prior to the correlation calculation, dispersive effects have been removed from the BPM data. This was achieved by identifying the dispersive modes with the help of a singular value decomposition (SVD), and subsequently removing the corresponding motion from the data via a decorrelation procedure. The removed dispersive orbit jitter was small. After the dispersion removal the RMS orbit jitter in horizontal direction was only reduced by 1.8% on average and by 4.8% at maximum. Vertically, the RMS orbit jitter reduction was 1.0% on average and 2.9% at maximum.

The results of the correlation of the predicted and measured orbit jitter are shown in Fig. 12. Correlations as high as 0.26 horizontally and 0.80 vertically can be observed if the technique to remove the incoming orbit jitter [introduced in Eqs. (16)–(18)] is not applied to the

BPM data. Even some strip line BPMs show correlation values clearly above the noise level. If the removal technique is applied, the correlation reduces drastically, which suggests that the main orbit jitter source is located upstream of the high-resolution cavity BPMs (located around sensor 6 and 7) used by the technique. This was expected after the ground motion analysis in Sec. IV B. These results are in strong contrast to the simulation results, where lower correlations have been predicted when no jitter reduction is applied. This discrepancy is due to the vibration source around sensor 2. The origin of the vibration source will be investigated in the next section. It is also interesting to note that the correlation results of the experiment in vertical direction with the application of the jitter removal technique (correlation coefficients of 0.22 in the final focus region) are very similar to the expectations from the simulations depicted in Fig. 6. This correlation in the measurements is however not due to the effect of other quadrupole magnets, but due to orbit jitter created by source 2, which has not been removed by the jitter removal procedure. This can be verified by not including the data from sensor 2 in the data evaluation.

The correlation of the predicted and measured orbit jitter data is also visible in frequency space, as depicted in Fig. 13. Since the beta function is significantly higher at BPM 30 compared to BPM 19, also the orbit jitter is higher. The PSDs of the predicted and measured data fit better for BPM 19, which was expected since the measured correlation coefficient in Fig. 12 is significant higher for BPM 19 than for BPM 30. If the two peaks at 9.94 Hz and 24.25 Hz in the ground motion PSD of sensor 2 in Fig. 9 are downsampled by the beam
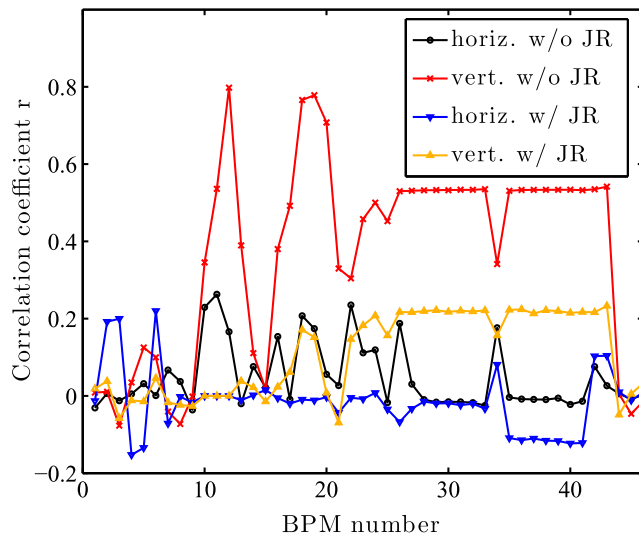

FIG. 12. Correlation coefficient calculated from the BPM measurements and the predictions from the ground motion sensors. The results are shown with and without removing the incoming orbit jitter (JR).
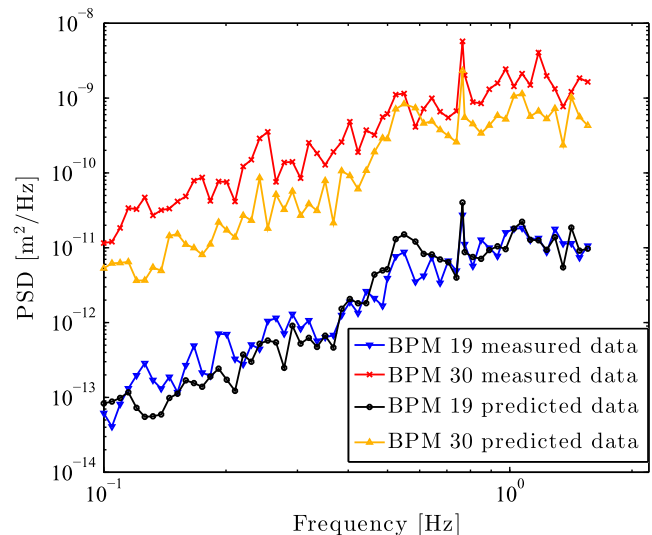

FIG. 13. Power spectral densities of the BPM measurements and the predictions from the ground motion sensors in vertical direction for the BPMs 19 and 30.

repetition rate of 3.124 Hz, they are located at aliasing frequencies of 0.56 Hz and 0.74 Hz. At these aliasing frequencies, an increase of the PSDs of the predicted and measured BPM data can be observed in Fig. 13. This is a further indication for the high correlation between the data sets.

In summary, it can be stated that the feasibility study of the prediction of orbit changes from ground motion measurements was successful. The prediction quality was better than initially expected thanks to a strong vibration source that was not included in the model. It is assumed that the observed correlation values are limited due to orbit jitter from other dynamic imperfections. No indications were found that there are any principle or practical problems that would prohibit the implementation of the system.

D. Orbit jitter reduction

A careful data analysis has shown that most of the orbit jitter due to ground motion originates from the region around sensor 2, which is located on top of QD2X. At a detailed inspection of the beam line, two vibration sources could be identified. The first source was a metal pipe that was touching a leg of the girder of QD2X. The pipe transports cooling water and vibrations were transmitted from the pipe to the girder. The second source was a plastic tube also transporting cooling water. It was mounted in the cable tray above QD2X, but got lose and was hanging down. It was not touching QD2X directly, but a dipole that is mounted on the same girder.

Both vibration sources were removed, and as a result the orbit jitter level in vertical direction was reduced by about a factor of 1.4, as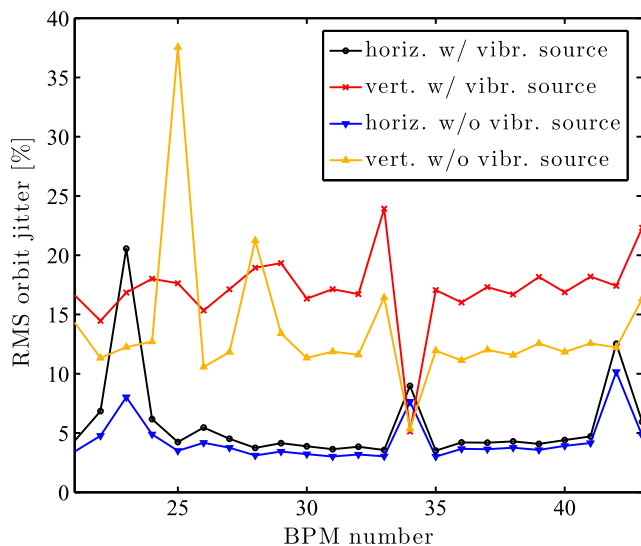 depicted in Fig. 14. It can be claimed that half of the jitter sources have been removed, since a reduction of the amplitude by a factor 1.4 corresponds to halving the orbit jitter power if the jitter sources are assumed to be independent of each other. The RMS orbit jitter values of the different BPMs are quite consistent, with the exceptions of BPM 23 in horizontal and BPM 25 in vertical direction. The increased orbit jitter in these two BPM measurements is due to some spikes in the data, which are not observable in the data of the adjacent BPMs. It is therefore assumed that these spikes are measurement artefacts of unknown origin. Also the observed RMS orbit jitter values in BPM 34 differ strongly from the values observed in the other BPMs. This deviation can be explained by the specific location of BPM 34, which is in a region of very small beta functions. Because of these small beta functions, the beam oscillations are also small and the noise content in the corresponding measurements is large, and the relative beta function measurement at this location has a high relative error.

The result of the vibration source removal is also clearly visible in the correlation plot in Fig. 15, where the measured and predicted orbit jitter data points at BPM 19 (MQF11X), i.e., ΔB_{19} and $\Delta \hat{B}_{19}$, are plotted. With the vibration source a clear correlation between the two data sets is visible. After the removal, the correlation is strongly reduced, but still visible. A week after these measurements, a second set of measurements was performed, which confirmed the reduction of the RMS orbit jitter. This shows that the feed-forward scheme is not only useful to suppress beam oscillations but also to identify error cases and to improve the site-specific ground motion knowledge. From Fig. 15 it is also clear that there is a

FIG. 14.   RMS orbit jitter relative to the beam size before and after the removal of the vibration sources.
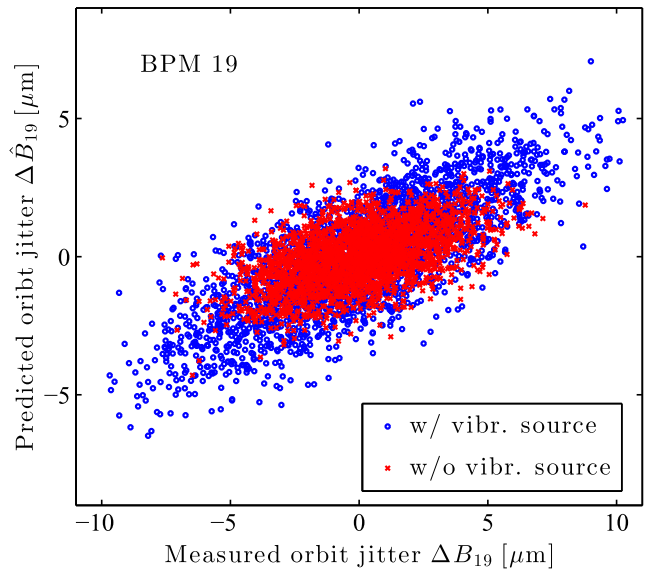

FIG. 15.   Predicted and measured orbit jitter at BPM 19, before and after the removal of the vibration sources.

scaling error between the measured and predicted data, which is due to a model mismatch. Such scaling errors will be a problem for the planned correction of the predicted data and have to be addressed in future work.

V. CONCLUSIONS AND FUTURE WORK

Ground motion is a severe problem for the operation of future linear colliders. For that reason, a novel mitigation scheme is presented, which uses a distributed ground motion measurement system to perform feed-forward control. It is able to damp orbit oscillations of higher frequency than orbit feedback systems can access. With respect to stabilization systems, it is significantly cheaper and easier to integrate into accelerator modules. In contrast to intratrain feedback systems, it is a global scheme that can correct distributed ground motion effects. In general, the global structure of the scheme allows for better optimized correction algorithms and error detection mechanisms that make the system more robust. However, the presented scheme will have higher demands on the control system and the corrector dynamics.

An analytical model has been developed for deriving hardware specifications and performance estimates of this system for a specific accelerator and ground motion model. Experimental studies at ATF2 have been performed, which prove the feasibility of the prediction of orbit changes due to ground motion. Surprisingly, a correlation as high as 80% between the predicted and measured orbit jitter has been observed. In the course of these studies, an orbit jitter source could be identified. Its removal halved the orbit jitter power at ATF2. This shows that the feed-forward scheme has also great potential to discover complex installation issues and model mismatches. Following up this work, the obtained orbit predictions will be used to correct the ground motion effects in a feed-forward fashion. Such a full system implementation is planned in the near future at ATF2.

ACKNOWLEDGMENTS

[1] V. Shiltsev, Phys. Rev. Lett. **104**, 238501 (2010).
[2] A. Sery and O. Napoly, Phys. Rev. E **53**, 5323 (1996).
[3] K. Kubo, Phys. Rev. ST Accel. Beams **14**, 014401 (2011).
[4] T. O. Raubenheimer, Phys. Rev. ST Accel. Beams **3**, 121002 (2000).
[5] T. Himel, Annu. Rev. Nucl. Part. Sci. **47**, 157 (1997).
[6] D. Bulfone, in *Proceedings of the 11th European Particle Accelerator Conference, Genoa, Italy, 2008* (EPS-AG, Geneva, 2008).
[7] CLIC Conceptual Design Report, Vol. 3, CERN Technical Report No. CERN-2012-007, 2007.
[8] R. Tomás, Phys. Rev. ST Accel. Beams **13**, 014801 (2010).
[9] International Linear Collider Reference Design Report, Vol. 3, ILC Technical Report No. ILC-Report-2007-001, 2007.
[10] ATF2 Proposal, KEK Technical Report 2005-2, 2006.
[11] G. White *et al.* (ATF2 Collaboration), Phys. Rev. Lett. **112**, 034802 (2014).
[12] J. Resta-López, P. Burrows, and G. Christian, JINST **5**, P09007 (2010).
[13] D. Schulte, in *Proceedings of the 26th Advanced ICFA Beam Dynamics Workshop on Nanometer Size Colliding Beams (Nanobeam 2002),* http://icfa-nanobeam.web.cern.ch/icfa-nanobeam/slides2.htm, pp. 61–67.
[14] C. Montag, Nucl. Instrum. Methods Phys. Res., Sect. A **378**, 369 (1996).
[15] C. Collette, S. Janssens, K. Artoos, A. Kuzmin, P. Fernandez-Carmona, M. Guinchard, R. Leuxe, and C. Hauviller, Nucl. Instrum. Methods Phys. Res., Sect. A **643**, 95 (2011).
[16] G. Balik, B. Caron, J. Allibe, A. Badel, J.-P. Baud, L. Brunetti, G. Deleglise, A. Jeremie, R. Le Breton, and S. Vilalte, J. Intell. Mater. Syst. Struct. **24**, 1785 (2013).
[17] A. Gaddi *et al.*, LCD-Note-2010-11, 2010.
[18] Y. Renier *et al.*, in *Proceedings of the 2012 International Particle Accelerator Conference (IPAC12)* (IEEE, New Orleans, 2012), TUPPR060.
[19] A. V. Oppenheim, R. W. Schafer, and J. R. Buck, *Discrete-Time Signal Processing*, 2nd ed. (Prentice Hall, Upper Saddle River, New Jersey, 1999).
[20] G. Franklin, J. D. Powell, and M. L. Workman, *Digital Control of Dynamic Systems* (Prentice Hall, Englewood Cliffs, NJ, 1997).
[21] J. Pfingstner, Ph.D. thesis, Vienna University of Technology, 2013.
[22] M. Günther, *Zeitdiskrete Steuerungssysteme* (VEB Verlag Technik, Berlin, 1988).
[23] Guralp Systems, CMG-6, http://www.guralp.com/products/instruments/cmg-6.
[24] S. Jannsens *et al.*, in *Proceedings of the 2nd International Particle Accelerator Conference, IPAC-2011, San Sebastián, Spain* (EPS-AG, Spain, 2011), TUPC014.
[25] C. Collete, S. Janssens, P. Fernandez-Carmona, K. Artoos, M. Guinchard, C. Hauviller, and A. Preumont, Bull. Seismol. Soc. Am. **102**, 1289 (2012).
[26] J. Snuverink *et al.*, in *Proceedings of the 2nd International Particle Accelerator Conference, IPAC-2011, San Sebastián, Spain* (EPS-AG, Spain, 2011), TUPC023.
[27] The Tracking code PLACET, https://savannah.cern.ch/projects/placet.
[28] ATF2 Flight Simulator, https://confluence.slac.stanford.edu/display/ATF/ATF2+Flight+Simulator.
[29] B. Bolzon *et al.*, in *Proceedings of the 23rd Particle Accelerator Conference, Vancouver, Canada, 2009* (IEEE, Piscataway, NJ, 2009), TH5RFP086.

[30] J. Pfingstner *et al.*, in *Proceedings of the 5th International Particle Accelerator Conference, IPAC-2014, Dresden, Germany* (EPS-AG, Dresden, 2014), TUPRO019.

[31] Octave, https://www.gnu.org/software/octave.

[32] Y. I. Kim *et al.*, Phys. Rev. ST Accel. Beams **15**, 042801 (2012).

[33] J. Irwin, C. Wang, Y. Yan, K. Bane, Y. Cai, F.-J. Decker, M. Minty, G. Stupakov, and F. Zimmermann, Phys. Rev. Lett. **82**, 1684 (1999).

[34] EPICS - Experimental Physics and Industrial Control System, Technical Report, http://www.aps.anl.gov/epics/.

[35] P. D. Welch, *IEEE Trans. on Audio Electroacoustics* **AU-15**, 70 (1967).